

SonoRank: Towards Calibration-Free Real-Time Finger Flexion Detection from Forearm Ultrasound Sequences

Dean Zadok¹, Alon Wolf², Alex M. Bronstein¹, Oren Salzman¹

Abstract—Powered prosthetic hands are frequently abandoned, largely due to the limited functionality of current devices that rely on surface electromyography (sEMG). Sonomyography (ultrasound) has emerged as a promising alternative, owing to its ability to observe muscle activity in real time and control a greater number of degrees of freedom. Yet, existing ultrasound-based methods require per-user fine-tuning, limiting their commercialization. We propose **SonoRank**, an important step towards calibration-free finger flexion detection from forearm ultrasound video. **SonoRank** first learns to rank pairs of ultrasound sequences by their relative motion magnitude for each of the five fingers. The learned representations are then fine-tuned to classify whether each finger is actively flexing, using a rest reference that is captured at the beginning of the operation. Under 12-fold leave-one-subject-out cross-validation on a dataset of twelve subjects with synchronized kinematics, **SonoRank** achieves a 28% improvement in F1 score over direct classification baselines that skip the ranking stage. These results establish pairwise ranking as an effective pretraining signal for subject-independent control, bringing ultrasound-based prosthetics closer to practical, calibration-free deployment.

I. INTRODUCTION

Six decades of prosthetics research have transformed artificial hands from simple grippers into mechatronic systems. Modern designs offer dozens of independent degrees of freedom, approaching human-level dexterity [1]. Yet 44% of upper-limb amputees reject their prostheses [2], suggesting a gap in the control interface. Since the mid-twentieth century, surface electromyography (sEMG) has remained the dominant non-invasive sensing modality for prosthetic hands [3], alongside plug-and-play interfaces [4]. However, sEMG captures only noisy electrical activity from superficial muscle fibers, making individual finger discrimination difficult [5]. Montagnani et al. showed that it is precisely finger dexterity that current prostheses lack [6], underscoring that the bottleneck lies mostly in sensing.

Ultrasound imaging of the forearm (i.e., sonomyography) offers a richer window into motor intent [7]. B-mode (brightness-mode) images, the grayscale cross-sections produced by conventional ultrasound, capture the spatial structure of deep muscles in real time, enabling the discrimination of finger movements from morphological deformations that sEMG cannot resolve [8], [9]. Yet existing sonomyography methods frame finger motion prediction as either discrete gesture classification [10], [11] or direct joint-angle regres-

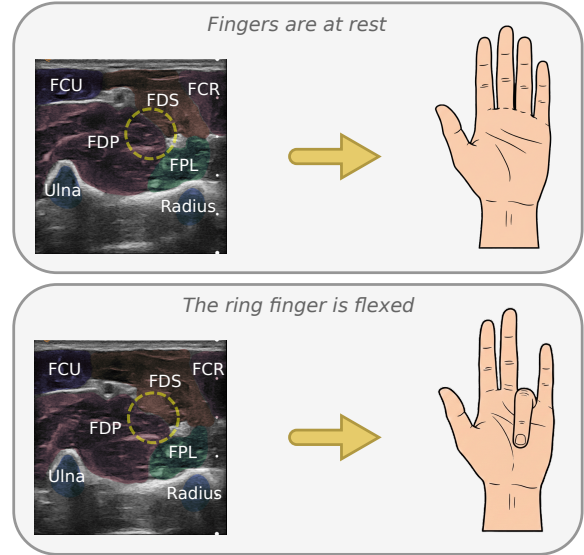


Fig. 1: Ultrasound can see what EMG cannot: B-mode cross-sections of the forearm (top of each image is the skin surface) at rest (top) and during ring-finger flexion (bottom), with the corresponding hand pose on the right. Muscle regions and bones were manually annotated for illustration purposes: the flexor digitorum superficialis (FDS) and profundus (FDP), the two extrinsic muscles that actuate the four fingers, are highlighted alongside the Ulna and Radius (blue). The dashed circle highlights the boundary between the FDS and FDP. During flexion, this region visibly deforms as the muscles contract and shift relative to each other. This morphological change is the signal that our method is designed to detect.

sion [9], [12]. Classification restricts output to a fixed gesture vocabulary, while regression demands subject-specific calibration of continuous kinematics labels [13]. Moreover, most approaches treat each finger independently, ignoring the biomechanical coupling among forearm muscles that actuate multiple fingers simultaneously [6]. Cross-subject generalization has so far been limited to A-mode armbands for wrist and hand tracking [14] or to systems that fuse ultrasound with surface electromyography [15]. The key question this work aims to answer is: *can we detect individual finger flexions from forearm ultrasound and instruct a robotic hand to replicate them, without calibration?*¹

Towards this goal, we propose **SonoRank**, which decomposes finger flexion detection into two training stages. First, a ranking model learns to compare pairs of ultrasound sequences by their relative motion magnitude for all five fingers independently. Because ranking compares relative motion rather than absolute measurements, the learned rep-

¹Department of Computer Science, Technion, Haifa, Israel {deanzadok,bron,osalzman}@cs.technion.ac.il

²Department of Mechanical Engineering, Technion, Haifa, Israel alonw@me.technion.ac.il

¹We do not showcase results on deformed muscles. We test on healthy subjects with fully functioning hands to provide an accurate benchmark for this task. Our code is available at github.com/deanzadok/sonorank.

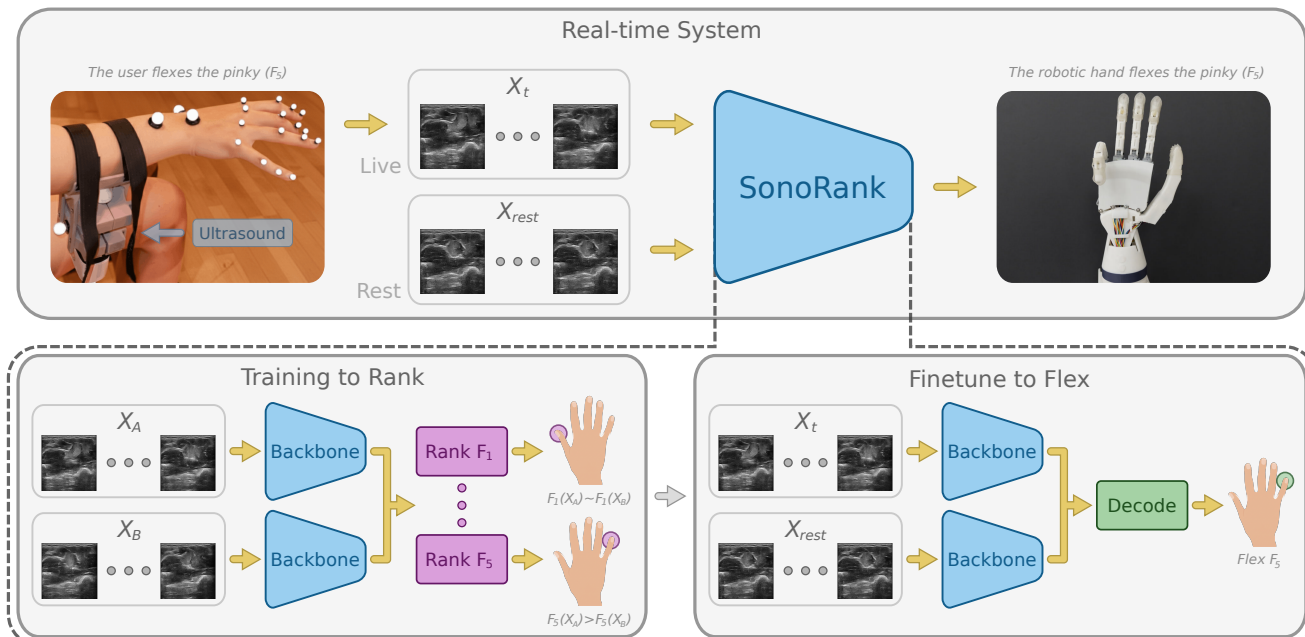


Fig. 2: Overview of the SonoRank framework. (Top) Real-time operation: a forearm ultrasound probe captures a live sequence X_t while the user flexes a finger. Together with a pre-recorded rest reference X_{rest} , both sequences are fed into SonoRank, which outputs per-finger flexion decisions that drive a robotic hand. (Bottom left) Stage 1, training to rank: two ultrasound sequences X_A and X_B are encoded through a shared backbone, and five parallel ranking heads (one per finger, F_1, \dots, F_5) learn to predict which sequence exhibits greater flexion for each finger. (Bottom right) Stage 2, fine-tuning to flex: the ranking heads are replaced by a classification head (Decode) that receives the concatenated embeddings of X_t and X_{rest} and predicts which fingers are actively flexing.

representations generalize across forearm morphologies without calibration. A second stage then fine-tunes the model to decide, for each finger, whether it is actively flexing. To the best of our knowledge, this is the first work to use pairwise ranking as a pretraining signal for subject-independent finger flexion detection from forearm ultrasound. Our contributions are: (i) A framework for cross-subject finger flexion detection from forearm ultrasound that requires no user-specific data or fine-tuning at deployment, (ii) A pairwise ranking formulation for sonomyography that learns subject-independent motion representations by comparing flexion magnitudes, avoiding calibration across different forearm morphologies, and (iii) Lessons learned from offline and online studies on experimenting with a calibration-free robotic system for the first time. Under 12-fold leave-one-subject-out cross-validation, SonoRank improves over direct classification baselines and outperforms all external methods by a wide margin, while running in real time on affordable GPUs.

II. RELATED WORK

Sonomyography has progressed from initial feasibility to wearable real-time systems over the past fifteen years [7]. Castellini and Passig [8] first showed that forearm ultrasound features are linearly related to finger positions, and subsequent work demonstrated real-time gesture classification [10], [16], confirming that US matches or exceeds sEMG for finger discrimination [5]. Since then, sonomyographic control has been validated clinically in individuals with upper-limb loss [17], [18], extended to nine individual finger motions [11], and demonstrated for cross-participant hand tracking [14], [9]. Wearable probes [19], [20] and flexible

transducers [21] have moved the technology toward deployment, while parallel efforts address sensor-reattachment robustness [22], cross-subject transfer [23], ultra-low-power inference [24], and clinical prosthetic validation [25].

Single-frame approaches, including early sonomyographic prosthetic control systems [26], discard the temporal dynamics of muscle contraction visible in ultrasound video. In the broader biosignal literature, hybrid CNN-Transformer architectures have become a dominant paradigm for temporal decoding [27]. Zadok et al. [28], [29] introduced a temporal architecture with kinematic representations for predicting fine finger motions from ultrasound, while Jiang et al. [21] combined a flexible US transducer with a Sonomyography Transformer for simultaneous gesture and force recognition. In the EMG domain, Zhang et al. [30] estimated multiple joint kinematics simultaneously, and Weng et al. [31] demonstrated real-time fine finger motion decoding in amputees. Despite these advances, most methods frame finger motion prediction as classification or regression, without exploiting relative temporal comparisons.

Pairwise ranking formulations have found applications beyond their origins in information retrieval. Misra et al. [32] showed that temporal order verification in video provides a self-supervised signal for visual representation learning. In medical imaging, Li et al. [33] used Siamese networks with pairwise comparison against references to produce continuous disease severity scores, and Dong et al. [34] showed that ranking longitudinal MRI scan pairs by temporal order captures progressive brain atrophy. Pairwise ranking has also been applied to skill assessment and temporal

change detection in video [35], and to time-series forecasting, where temporal relational ranking outperforms pointwise regression [36]. Our work follows a similar motivation: we use pairwise temporal ranking as a supervised learning signal, comparing motion sequences against rest references to generalize across unseen forearm morphologies. To jointly predict all five fingers from a shared backbone, we adopt multi-task learning with a shared representation and per-finger loss balancing [37].

III. METHOD

We begin with the anatomy linking forearm ultrasound to finger motion. The forearm contains several extrinsic flexor muscles whose contractions are visible in B-mode ultrasound and directly control finger motion [38]. The flexor digitorum superficialis (FDS) and flexor digitorum profundus (FDP) actuate the index, middle, ring, and pinky fingers through tendons that cross the proximal interphalangeal (PIP) and distal interphalangeal (DIP) joints, respectively, while the flexor pollicis longus (FPL) controls the thumb. Because the FDS and FDP share tendons across the four fingers, flexing one finger produces morphological changes that overlap with those of neighboring fingers, making per-finger discrimination challenging (Fig. 1). The FPL is one of the smallest extrinsic flexors, and the primary thumb muscles (the thenar group) lie in the palm, outside the ultrasound field of view, which complicates thumb prediction. These anatomical constraints motivate a shared multi-finger and temporal representation that can learn the coupled muscle dynamics.

A. Problem Definition

Let $x_t \in \mathbb{R}^{H \times W}$ denote a B-mode ultrasound image of the forearm acquired at time t (see Fig. 2). For each finger $f \in \mathcal{F} = \{F_1, \dots, F_5\}$ (thumb, index, middle, ring, pinky), let $\theta_{MP,t}^{(f)}$ and $\theta_{PIP,t}^{(f)}$ denote its metacarpophalangeal and proximal interphalangeal joint angles at time t , and define the total flexion angle as $\theta_t^{(f)} = \theta_{MP,t}^{(f)} + \theta_{PIP,t}^{(f)}$. A temporal sequence $X = \{x_1, \dots, x_T\}$ consists of T consecutive frames from a recording trial. We define the motion magnitude of finger f over the sequence as the absolute change in flexion angle:

$$\delta^{(f)}(X) = |\theta_T^{(f)} - \theta_1^{(f)}|. \quad (1)$$

Our goal is to predict whether each finger is actively flexing within a window of frames. We decompose this problem into two stages: a pairwise ranking model that learns motion dominance for each finger from pairs of sequences (Sec. III-B), and a classifier that predicts finger flexion from the learned representations (Sec. III-C). We refer to the combined two-stage system as **SonoRank**.

B. Pairwise Temporal Ranking

Rather than predicting flexion labels directly, we first train a model to compare temporal sequences by their relative motion magnitude. Given two sequences X_A, X_B from the same trial, the ranking label for finger f is

$$y^{(f)} = \mathbf{1}[\delta^{(f)}(X_A) > \delta^{(f)}(X_B)]. \quad (2)$$

Additionally, a pair is *informative* for finger f only when the motion difference exceeds a minimum threshold τ_{\min} :

$$m^{(f)} = \mathbf{1}[|\delta^{(f)}(X_A) - \delta^{(f)}(X_B)| \geq \tau_{\min}], \quad (3)$$

with $\tau_{\min} = 3^\circ$ in all experiments. The ranking model (Fig. 2, bottom left) consists of a shared encoder that maps each ultrasound frame to a feature vector, a temporal transformer module that aggregates frame-level features into a sequence-level embedding, and five parallel comparison heads (one per finger f) that each produce the ranking probability

$$\hat{p}^{(f)} = P(\delta^{(f)}(X_A) > \delta^{(f)}(X_B) \mid X_A, X_B). \quad (4)$$

The shared encoder and transformer capture dynamics common to all fingers, while each comparison head specializes in the motion pattern of each finger. The training objective combines binary cross-entropy (ℓ_{BCE}) on informative pairs with an uncertainty penalty on uninformative ones:

$$\mathcal{L}_{\text{rank}} = \frac{1}{|\mathcal{F}|} \sum_{f \in \mathcal{F}} [m^{(f)} \ell_{\text{BCE}}^{(f)} + \lambda (1 - m^{(f)}) (\text{logit}^{(f)})^2]. \quad (5)$$

The first term trains the model to rank correctly when sufficient motion difference exists. The second term is an *uncertainty penalty* applied when the finger f is inactive ($m^{(f)}=0$). The squared logit pushes predictions toward $\hat{p}=0.5$, preventing the model from learning unwanted rankings on pairs where motion ordering is ambiguous. This ranking formulation avoids subject-specific calibration, as comparing which sequence exhibits more motion generalizes across morphologies.

In inference (Fig. 2, top), the second sequence is fixed to a known rest reference X_{rest} (where the fingers are idle) and X_t slides through the recording, yielding for each finger f a continuous signal $\hat{p}_t^{(f)} = P(\delta^{(f)}(X_t) > \delta^{(f)}(X_{\text{rest}}) \mid X_t, X_{\text{rest}})$. While this signal captures relative flexion magnitude, it does not directly indicate whether a finger is actively flexing, and a second stage is needed to turn the learned representations into real-time flexion decisions.

C. Flexion Classification

After ranking pretraining, we discard the five comparison heads and replace them with a classification head (Fig. 2, bottom right): a multi-layer perceptron (MLP) that maps sequence-level embeddings to five binary flex predictions. Given a query sequence X and a rest reference X_{rest} , both are encoded through the shared backbone (frame encoder, temporal transformer, and mean pooling) to produce sequence-level embeddings e and e_{rest} . The concatenated vector $[e, e_{\text{rest}}]$ is passed through the MLP, which outputs a flex prediction $\hat{y}^{(f)} \in [0, 1]$ for each finger f . Because the five predictions are produced independently rather than through a single mutually exclusive choice, the model can in principle represent several fingers flexing simultaneously. The entire model, including the pretrained backbone, is fine-tuned end-to-end with ℓ_{BCE} against ground-truth flex labels derived from the joint kinematics, where $y^{(f)} \in \{0, 1\}$ is the majority-vote flex label for finger f over the frames in the

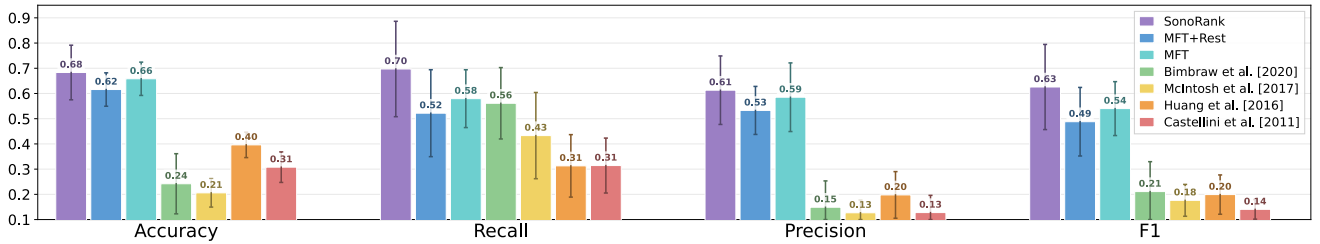


Fig. 3: Accuracy, recall, precision, and F1 score for seven methods under 12-fold leave-one-subject-out evaluation (error bars: ± 1 std across folds). The first three methods are ours: SonoRank (full pipeline), MFT+Rest (no ranking pretraining), and MFT (no ranking, no rest reference). The remaining four are external baselines reimplemented on our dataset [5], [8], [10], [12]. SonoRank leads consistently across all four metrics, while external baselines achieve F1 scores of 0.21 or lower, showing that single-frame classifiers and hand-crafted features fail to generalize across subjects.

query window. At inference, the window slides through the recording one frame at a time, producing a per-frame flexion decision for each finger. This two-stage design separates representation learning from classification. Ranking teaches the backbone motion-sensitive features that generalize across subjects, and fine-tuning adapts them for flex detection.

IV. EXPERIMENTAL SETUP

Our setup includes a Clarius L15HD (wireless B-mode ultrasound device) and a Vicon motion-capture system. The ultrasound was configured for the musculoskeletal (MSK) mode at 20 MHz, generating 480×480 images at 19 to 21 frames per second. The probe was attached to the forearm in the “transverse” orientation using a wearable strap [10]. The Vicon system tracked reflective markers on the hand, from which joint angles across five fingers were extracted via a forward kinematic model [13] (Appendix A). Ultrasound images were downsampled to 224×224 and subsampled by a factor of two, yielding an effective rate of approximately 10 Hz. We collected data from twelve right-handed subjects (seven men and five women, average age 23), all without neurological disorders or hand deformities. Each subject completed three enrollment sessions of isolated finger flexions, with three to five recordings of approximately ninety seconds each and rest periods in between. The final dataset comprises 51 recordings totaling approximately 84,000 ultrasound frames with synchronized kinematics. The study was approved by the institution’s Ethics Committee.

In all evaluations, we use 12-fold leave-one-subject-out cross-validation. In each fold, one subject serves as the test set, the preceding subject as the validation set, and the remaining ten subjects form the training set. The primary metric is per-finger area under the ROC curve (AUC), computed on active pairs ($m^{(f)}=1$). We report mean AUC across the five fingers as the aggregate measure. Training and optimization details are provided in Appendix B.

V. RESULTS

We first analyze SonoRank through a series of ablations (Sec. V-A): a comparison against direct classification baselines, an evaluation of different window lengths, and per-finger and per-subject breakdowns. We then evaluate real-time inference throughput (Sec. V-B).

A. Ablation Study

How important is ranking for generalizing to unseen subjects? We isolate the contribution of the ranking-pretrained backbone and the rest reference by comparing SonoRank against two baselines (Fig. 3). All three share the same architecture and initialize the image encoder from a model pretrained on image reconstruction [39]. MFT (Multi-Frame Transformer) trains the classifier directly on the pretrained encoder from the live sequence alone, and MFT+Rest additionally receives the rest reference. Both skip the pairwise ranking stage that distinguishes SonoRank.

SonoRank achieves F1 of 0.63, outperforming both MFT (0.54) and MFT+Rest (0.49), demonstrating the value of ranking pretraining. A Wilcoxon signed-rank test yields $p=0.065$ with a 95% CI of the mean difference of $[+0.001, +0.182]$. That MFT+Rest does not benefit from the rest reference without ranking pretraining indicates that the two components are synergistic. The backbone must learn *how* to compare against rest for the reference to be useful. Fig. 4 illustrates this on four test subjects: SonoRank produces sharper, better-aligned detections, while baselines miss events or generate fragmented predictions. Inter-subject variability remains high (F1 from 0.46 to 0.83, $\sigma=0.11$), underscoring the difficulty of cross-subject generalization.

To put the absolute performance of SonoRank into context, we compare against four sonomyography methods reimplemented on our dataset under the same leave-one-subject-out protocol (Fig. 3). Castellini and Passig [8] extract features from circular image patches and predict finger positions with Ridge regression. Huang and Liu [5] sample pixel-intensity columns and classify finger states with a two-layer MLP. McIntosh et al. [10] (EchoFlex) compute dense optical flow between consecutive frames and pool the resulting field for MLP classification. Bimbraw et al. [12] classify individual frames using a modified VGG16. All four achieve F1 of 0.21 or lower on unseen subjects. We also evaluated the CBMF model [28], [29], but its training collapsed to constant outputs and was excluded. Even MFT, our weakest variant, outperforms all external baselines by a wide margin (accuracy 0.66 vs. 0.40), suggesting that multi-frame temporal modeling is a primary driver of cross-subject generalization. The remaining ablations evaluate the ranking backbone directly using per-finger AUC, as the ranking stage determines the quality of the representations that the classifier builds upon.

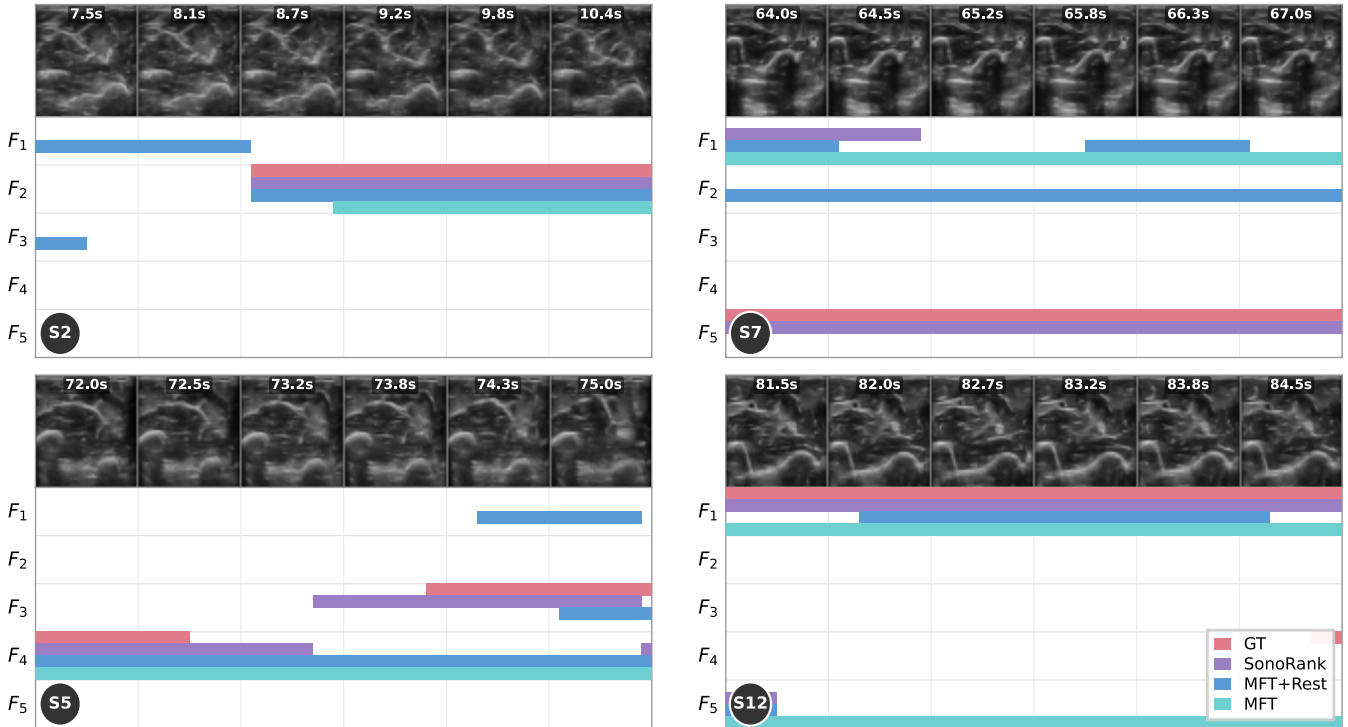


Fig. 4: Representative examples of finger flexion predictions on four test subjects. Each panel shows six ultrasound frames spanning a 3 s flexion interval (top) and the corresponding ground-truth and predicted flex labels for all five fingers (bottom). (Top-left) S2: clean F_2 (index) detection. SonoRank matches the ground truth perfectly while baselines produce shorter or misaligned events. (Top-right) S7: F_5 (pinky) flexion that SonoRank detects but both MFT+Rest and MFT miss entirely. (Bottom-left) S5: coupled F_3/F_4 (middle/ring) flexion. SonoRank captures the dominant fingers but adds a spurious F_4 event. (Bottom-right) S12: F_1 (thumb) flexion, the hardest finger. All methods detect the event, yet SonoRank aligns most closely with the ground truth.

How much temporal context is needed to capture finger flexion? To evaluate the effect of context length on ranking quality, we measure per-finger AUC across different window durations T (Fig. 5a). Performance climbs steeply from $T=0.15$ s (2 frames) through $T=0.75$ s (8 frames) and peaks at $T=1.55$ s (16 frames), roughly spanning one flexion-extension cycle. Extending to $T=2.35$ s (24 frames) yields no further gain, and longer windows were infeasible due to GPU memory constraints. The per-finger breakdown reveals an interesting reversal: at $T=0.15$ s F_1 (thumb) is the easiest finger to discriminate (0.68) while F_2 (index) is the hardest (0.55), yet at $T=1.55$ s this ranking inverts, with F_2 reaching 0.71 and F_1 dropping to 0.67. We attribute this to the quicker flexion motion of F_1 , which is easier to capture in a shorter window, whereas the other fingers produce longer motions that benefit from longer context.

How does prediction difficulty vary across subjects and fingers? Fig. 5c reveals large inter-subject variability: the top four subjects (S5, S9, S12, S2) average 0.76, while the bottom four (S11, S3, S7, S8) average 0.61. We attribute this spread to differences in forearm morphology and subject performance during data collection. Averaged across subjects, F_2 (index) is the easiest finger to predict (0.71), followed by F_4 (ring) and F_5 (pinky) whose shared FDP tendons cause overlapping ultrasound signatures, while F_1 (thumb) ranks lowest (0.67). We attribute this gap to F_1 anatomy (Sec. III): its extrinsic flexor (FPL) is one of the smallest muscles in

the image, and the primary thumb flexors lie in the palm, outside the ultrasound field of view. Nevertheless, finger difficulty varies across subjects: F_1 is the top-performing finger for S1 (0.82) yet the weakest for S4 (0.58), indicating that individual anatomy and flexing behavior affect which fingers are easiest to decode.

How many subjects are needed for the ranking model to generalize? Fig. 5b shows ranking AUC as a function of the number of training subjects. Performance rises steeply from one subject (0.55) to three (0.64). However, adding subjects beyond five yields only marginal gains, with the entire set of ten subjects reaching 0.69. This suggests that approximately five subjects already capture sufficient forearm morphology diversity for the ranking model to generalize. This is an encouraging finding for practical deployment where data collection is costly.

B. Real-Time System Performance

To demonstrate that SonoRank can operate in real time, we built an end-to-end system (Fig. 6) connecting a Clarius L15HD ultrasound probe to a robotic hand [1] via a PC running inference. The demonstration was performed with a new user who did not participate in the offline data collection and had no prior experience operating the system. The startup procedure requires only that the user hold their hand relaxed for two to three seconds. During this brief period, the system captures a single rest frame, which is duplicated $T=16$ times to form the rest reference X_{rest} that remains fixed for the

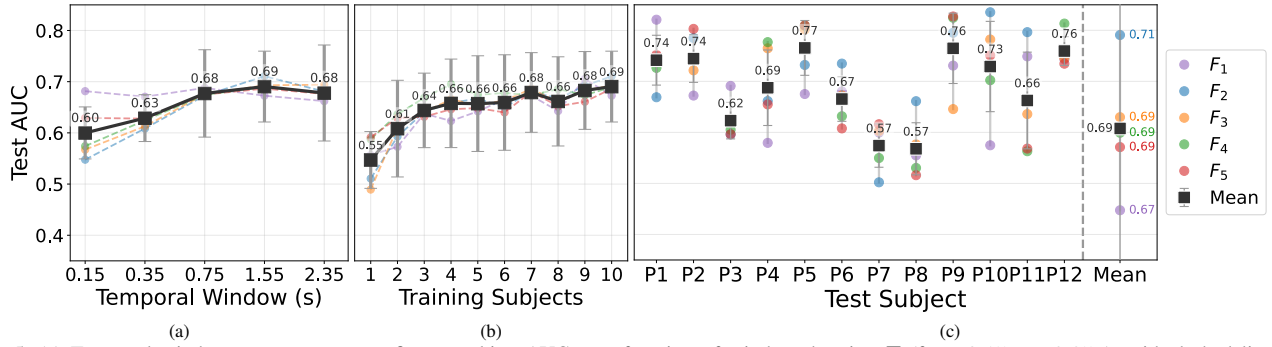


Fig. 5: (a) Temporal window sweep: mean per-finger ranking AUC as a function of window duration T (from 0.15 s to 2.35 s), with dashed lines for individual fingers and black squares for mean values (± 1 std). (b) Training set size: ranking AUC as a function of the number of training subjects, showing that adding more than five subjects yields diminishing returns. (c) Per-subject ranking performance: each column shows per-finger AUCs (colored dots: $F_1 - F_5$) and mean (black square). F_2 (index) leads at 0.71, F_1 (thumb) trails at 0.67, overall mean 0.69. All panels report mean ranking AUC averaged over 12 leave-one-subject-out folds.

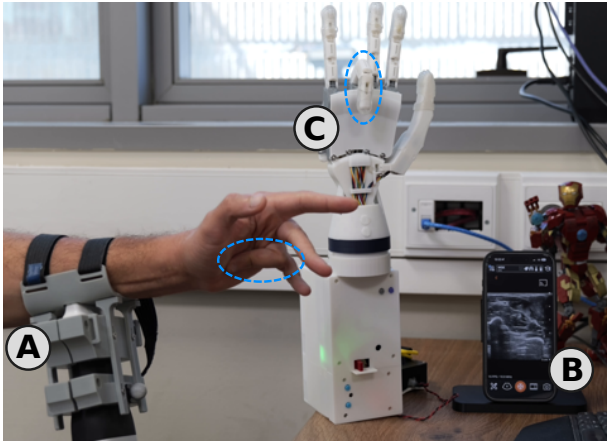


Fig. 6: Real-time demonstration of the SonoRank system. (A) Clarius ultrasound probe mounted on the forearm with a 3D-printed holder. (B) Smartphone displaying the live ultrasound feed (for visualization only). Frames are streamed directly from the probe to the PC. (C) Robotic hand [1] mirroring the detected finger flexion in real time.

entire session. Simultaneously, the sliding buffer of 31 raw frames fills as the probe streams at 20 Hz, and the model observes the baseline per-finger probabilities during rest to automatically set activation thresholds. Once the buffer is full, each new frame triggers a forward pass that produces five per-finger flex probabilities. The system selects the single most confident finger above its threshold and sends a command to the robotic hand, filtering brief fluctuations to ensure stable control.

As for model latency, we benchmarked the inference pipeline on a consumer-grade NVIDIA RTX 3080 using pre-recorded H5 sessions. The full model has 10.7 million parameters, and a single forward pass takes 17.5 ms on average, corresponding to 57 Hz, nearly three times the 20 Hz ultrasound frame rate. Because the classifier is trained with majority-vote labels, a flexion is typically detected once roughly half the window contains flexion frames, yielding an estimated detection delay of ~ 0.78 s. This delay can be reduced to ~ 0.39 s by halving the temporal window, which retains ranking performance (Fig. 5a). In practice, the observed algorithmic delay was ~ 0.5 s, confirming real-time operation. Note that the actuation delay, which depends on

the robotic platform, is added on top. Since our method requires only an update rate of 10 Hz, the computational prediction budget is 100 ms, leaving plenty of room for deployment on embedded platforms. Techniques such as half-precision inference and model pruning can reduce latency further without modifying the architecture.

VI. DISCUSSION AND FUTURE WORK

We presented SonoRank, a two-stage approach for detecting per-finger flexion from forearm ultrasound without subject-specific calibration. The results show that temporal modeling and pairwise ranking are complementary drivers of cross-subject generalization: temporal context alone (MFT) already outperforms external baselines, while the ranking-pretrained backbone combined with a rest reference (SonoRank) lifts macro F1 to 0.63, roughly three times that of the best external baseline. The model runs at 57 Hz on a consumer-grade GPU with sub-second detection delay (Sec. V-B). These results notwithstanding, several limitations remain. The study is limited to twelve healthy, right-handed subjects performing isolated single-finger flexions in a controlled setting. Inter-subject variability is high (F1 scores from 0.46 to 0.83, $\sigma=0.11$), and F_1 (thumb) is consistently the hardest finger to detect, likely because its primary flexors reside in the palm and are invisible to forearm ultrasound (Fig. 5c).

This variability indicates that current accuracy is not yet sufficient for production. Defining a minimal performance threshold, below which the system requests a calibration session, could close this gap while preserving calibration-free operation for most users. Beyond prosthetics, calibration-free finger detection can enable engagement with digital devices [40], musical instruments [16], gaming [41], and virtual reality [14] without per-session setup. Most importantly, because the ranking formulation learns relative motion comparisons rather than absolute patterns, it is well-suited for generalization to individuals with upper-limb amputations, whose residual muscle structure differs from intact forearms. Validating this is the next step toward intuitive and calibration-free prosthetic finger control.

ACKNOWLEDGMENT

We thank Haifa3D for their generous support and shared vision of accessible assistive technology. This project has received funding from the Israeli Ministry of Science & Technology (grant No. 8774), the David Himelberg Foundation, and the Wynn Family Foundation.

APPENDIX

A. Label Processing

The joint angles used to define flexion labels are computed from reflective hand markers tracked by a Vicon motion-capture system (Fig. 7). Each marker provides a 3D position, and we denote the vector from marker a to marker b as $\vec{v}_{a \rightarrow b} = \vec{b} - \vec{a}$. The angle at a joint is computed from two vectors sharing a common vertex using the two-argument arctangent:

$$\angle(\vec{u}, \vec{v}) = \text{atan2}(\|\vec{u} \times \vec{v}\|_2, \vec{u} \cdot \vec{v}). \quad (6)$$

Each of the four fingers (F_2 to F_5) has three anatomical joints: metacarpophalangeal (MP), proximal interphalangeal (PIP), and distal interphalangeal (DIP). In this work, we compute only the MP and PIP angles, as these two joints capture the dominant flexion motion. Using the little finger (F_5) as an example, with markers f_{41} (MP), f_{42} (PIP), and f_{43} (DIP tip), and t_5 on the metacarpal:

$$\begin{aligned} \theta_{\text{MP}}^{(F_5)} &= \angle(\vec{v}_{f_{41} \rightarrow t_5}, \vec{v}_{f_{41} \rightarrow f_{42}}), \\ \theta_{\text{PIP}}^{(F_5)} &= \angle(\vec{v}_{f_{42} \rightarrow f_{41}}, \vec{v}_{f_{42} \rightarrow f_{43}}). \end{aligned} \quad (7)$$

The thumb (F_1) is handled differently because its pressing motion is not well described by the same planar angles. The interphalangeal joint $\theta_{\text{PIP}}^{(F_1)}$ is the angle at marker t_6 between $\vec{v}_{t_6 \rightarrow t_7}$ and $\vec{v}_{t_6 \rightarrow t_5}$, while the MP joint $\theta_{\text{MP}}^{(F_1)}$ is the angle between $\vec{v}_{t_5 \rightarrow t_6}$ and the normal \hat{n}_p to the palm plane, estimated from markers f_{11} , f_{41} , and t_4 .

The total flexion angle for finger f is $\theta_t^{(f)} = \theta_{\text{MP},t}^{(f)} + \theta_{\text{PIP},t}^{(f)}$ (Sec. III-A). A frame is labeled as flexing if $\theta_t^{(f)}$ exceeds a threshold derived from each finger’s range of motion during the session. For the ranking stage, the motion magnitude $\delta^{(f)}(X)$ (Eq. 1) provides the pairwise labels. For the classification stage, the per-sequence flex label is the majority vote over frames in the window.

B. Model Implementation

All three models evaluated in Sec. V-A (SonoRank, MFT+Rest, and MFT) share the same backbone architecture. The backbone consists of a frame encoder followed by a temporal transformer. The frame encoder is a five-stage convolutional network with residual connections. The first stage applies a 7×7 convolution with stride 2 to the 224×224 input, producing 64 feature maps with a residual block, stages 2 to 4 each downsample with stride-2 convolutions and double the channel count (128, 256, 512) with residual blocks, and stage 5 applies a final stride-2 convolution (512 channels). Global average pooling and a linear layer project the resulting feature map to a 64-dimensional embedding

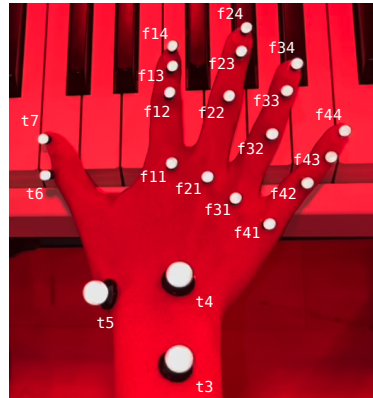


Fig. 7: Position of each reflective marker on the subject’s hand, as tracked by the Vicon motion-capture system.

vector. Each frame in the input sequence is encoded independently using the same shared weights. The sequence of frame embeddings is then summed with a learnable positional encoding and passed through a Transformer encoder with 2 layers, 4 attention heads, a feed-forward dimension of 256, and pre-layer normalization. Mean pooling over the output sequence yields a 64-dimensional embedding of the input window’s temporal dynamics.

In SonoRank, the backbone is first trained with five parallel ranking heads (Sec. III-B). Each ranking head is a four-layer MLP ($128 \rightarrow 256 \rightarrow 128 \rightarrow 64 \rightarrow 1$) with ReLU and dropout, mapping the concatenated embeddings of two sequences to a scalar logit $P(\text{flex}_A > \text{flex}_B)$. After ranking pretraining, the five heads are replaced by a classification MLP ($128 \rightarrow 128 \rightarrow 64 \rightarrow 5$) mapping the concatenated query and rest embeddings to five independent flex probabilities (Sec. III-C). Only the classification head is initialized from scratch, and the full model is fine-tuned end-to-end.

MFT+Rest uses the same classification MLP and rest-reference input as SonoRank, but skips the ranking stage entirely: the backbone is initialized from an image-reconstruction pretraining, and the classifier is trained directly. MFT further removes the rest reference, so its classification MLP receives only the 64-dimensional query embedding ($64 \rightarrow 128 \rightarrow 64 \rightarrow 5$) and must predict flexion from the live sequence alone.

The ranking stage is trained for 10 epochs with a batch size of 8 and 5×10^4 virtual pair samples per epoch. We use the Adam optimizer with discriminative learning rates: 10^{-5} for early encoder layers, 5×10^{-5} for late encoder layers, 10^{-4} for the transformer, and 3×10^{-4} for the comparison heads, with cosine annealing. The uncertainty penalty coefficient (Eq. 5) is set to $\lambda=0.5$, selected via grid search over $\{0, 0.1, 0.25, 0.5, 1, 2\}$. The ranking performance was stable for $\lambda \leq 0.5$ and degraded for larger values. The classification stage then fine-tunes the full model end-to-end for 10 additional epochs. Dropout is set to 0.3 throughout. Geometric and intensity augmentations are applied consistently across all frames in each sequence to preserve temporal coherence. The full implementation, including training configurations, is available at github.com/deanzadok/sonorank.

REFERENCES

- [1] D. Zadok, T. Naamani, Y. Bar-Ratson, E. Barash, O. Salzman, A. Wolf, A. M. Bronstein, and N. Krausz, "Digiarm: An anthropomorphic 3d-printed prosthetic hand with enhanced dexterity for typing tasks," *arXiv preprint arXiv:2602.23017*, 2026.
- [2] S. Salminger, H. Stino, L. H. Pichler, C. Gstoettner, A. Sturma, J. A. Mayer, M. Szivak, and O. C. Aszmann, "Current rates of prosthetic usage in upper-limb amputees - have innovations had an impact on device acceptance?" *Disabil. Rehabil.*, vol. 44, no. 14, pp. 3708–3713, 2022.
- [3] P. Herberths, "Myoelectric signals in control of prostheses: Studies on arm amputees and normal individuals," *Acta. Orthop.*, vol. 40, no. suppl24, pp. 1–83, 1969.
- [4] D. Zadok, O. Salzman, A. Wolf, and A. M. Bronstein, "Smart ankleband for plug-and-play hand-prosthetic control," *arXiv*, vol. abs/2503.17846, 2025.
- [5] Y. Huang and H. Liu, "Performances of surface EMG and ultrasound signals in recognizing finger motion," in *HSI*, 2016, pp. 117–122.
- [6] F. Montagnani, M. Controzzi, and C. Cipriani, "Is it finger or wrist dexterity that is missing in current hand prostheses?" *IEEE Trans. Neural Syst. Rehabil. Eng.*, vol. 23, no. 4, pp. 600–609, 2015.
- [7] K. He, "Ultrasound-based human machine interfaces for hand gesture recognition: A scoping review and future direction," *IEEE Transactions on Medical Robotics and Bionics*, vol. 7, pp. 200–212, 2025.
- [8] C. Castellini and G. Passig, "Ultrasound image features of the wrist are linearly related to finger positions," in *IROS*, 2011, pp. 2108–2114.
- [9] B. G. Sgambato, M. H. Hasbani, D. Y. Barsakcioglu, J. Ibáñez, A. Jakob, M. Fournelle, M. Tang, and D. Farina, "High performance wearable ultrasound as a human-machine interface for wrist and hand kinematic tracking," *IEEE Trans. Biomed. Eng.*, vol. 71, no. 2, pp. 484–493, 2024.
- [10] J. McIntosh, A. Marzo, M. Fraser, and C. Phillips, "Echoflex: Hand gesture recognition using ultrasound imaging," in *CHI*, 2017, pp. 1923–1934.
- [11] Y. Lee, K. Ko, J. Jang, J.-M. Lee, and C. Yoon, "A deep learning framework for finger motion recognition using forearm ultrasound imaging," *Sci. Rep.*, vol. 15, p. 39719, 2025.
- [12] K. Bimbraw, C. J. Nycz, M. J. Schueler, Z. Zhang, and H. K. Zhang, "Simultaneous estimation of hand configurations and finger joint angles using forearm ultrasound," *IEEE Trans. Med. Robot. Bionics.*, vol. 5, no. 1, pp. 120–132, 2023.
- [13] P. Cerveri, E. D. Momi, N. Lopomo, G. Baud-Bovy, R. M. L. Barros, and G. Ferrigno, "Finger kinematic modeling and real-time hand motion estimation," *Ann. Biomed. Eng.*, vol. 35, pp. 1989–2002, 2007.
- [14] B. G. Sgambato, B. K. Hodossy, D. Y. Barsakcioglu, X. Yang, A. Jakob, M. Fournelle, M.-X. Tang, and D. Farina, "Virtual reality interactions via a user-generic ultrasound human-machine interface for wrist and hand tracking," *Nat. Commun.*, vol. 16, p. 11062, 2025.
- [15] S. Bastola, C. Huynh, A. Tekes, and C. Tekes, "Hybrid deep learning method for continuous 2-dof hand motion prediction using electromyography and ultrasound," in *IEEE SoutheastCon*, 2025, pp. 1221–1226.
- [16] C. Castellini, K. Hertkorn, M. Sagardia, D. S. González, and M. Nowak, "A virtual piano-playing environment for rehabilitation based upon ultrasound imaging," in *BioRob*, 2014, pp. 548–554.
- [17] A. S. Dhawan, B. Mukherjee, S. Patwardhan, N. Akhlaghi, G. Diao, G. Levay, R. Holley, W. M. Joiner, M. Harris-Love, and S. Sikdar, "Proprioceptive sonomyographic control: A novel method for intuitive and proportional control of multiple degrees-of-freedom for individuals with upper extremity limb loss," *Sci. Rep.*, vol. 9, no. 1, p. 9499, 2019.
- [18] V. Nazari and Y.-P. Zheng, "A highly efficient hmi algorithm for controlling a multi-degree-of-freedom prosthetic hand using sonomyography," *Sensors*, vol. 25, no. 13, p. 3968, 2025.
- [19] J. Yan, X. Yang, X. Sun, Z. Chen, and H. Liu, "A lightweight ultrasound probe for wearable human-machine interfaces," *IEEE Sens. J.*, vol. 19, no. 14, pp. 5895–5903, 2019.
- [20] X. Yang, Z. Chen, N. Hettiarachchi, J. Yan, and H. Liu, "A wearable ultrasound system for sensing muscular morphological deformations," *IEEE Trans. Syst. Man Cybern. Syst.*, vol. 51, no. 6, pp. 3370–3379, 2021.
- [21] X. Peng, Y. Liu, F. Tan, W. Chen, Z. Liu, T. Ma, X. Li, and G. Li, "A novel transformer-based approach for simultaneous recognition of hand movements and force levels in amputees using flexible ultrasound transducers," *IEEE Trans. Neural Syst. Rehabil. Eng.*, vol. 31, pp. 4580–4590, 2023.
- [22] X. Yang, D. Zhou, Y. Zhou, Y. Huang, and H. Liu, "Towards zero re-training for long-term hand gesture recognition via ultrasound sensing," *IEEE J. Biomed. Health Informatics*, vol. 23, no. 4, pp. 1639–1646, 2019.
- [23] Y. Lian, Z. Lu, X. Huang, Q. Shangguan, L. Yao, J. Huang, and Z. Liu, "A transfer learning strategy for cross-subject and cross-time hand gesture recognition based on a-mode ultrasound," *IEEE Sens. J.*, vol. 24, no. 10, pp. 17 183–17 192, 2024.
- [24] S. Vostrikov, M. Anderegg, L. Benini, and A. Cossetini, "Unsupervised feature extraction from raw data for gesture recognition with wearable ultralow-power ultrasound," *IEEE Trans. Ultrason. Ferroelectr. Freq. Control*, 2024.
- [25] S. M. Engdahl, S. A. Acuna, R. R. Kaliki, and S. Sikdar, "Sonomyography for control of upper-limb prostheses: Current state and future directions," *JPO: J. Prosthet. Orthot.*, vol. 36, no. 3, pp. 174–184, 2024.
- [26] K. Bimbraw, E. Fox, G. Weinberg, and F. L. Hammond, "Towards sonomyography-based real-time control of powered prosthesis grasp synergies," in *EMBC*, 2020, pp. 4753–4757.
- [27] A. Anwar, Y. Khalifa, J. L. Coyle, and E. Sejdic, "Transformers in biosignal analysis: A review," *Inf. Fusion*, vol. 114, p. 102697, 2025.
- [28] D. Zadok, O. Salzman, A. Wolf, and A. M. Bronstein, "Towards predicting fine finger motions from ultrasound images via kinematic representation," in *ICRA*, 2023, pp. 12 645–12 651.
- [29] —, "Inferring fine finger motions for prosthetic control: An ultrasound-based approach to real-time estimation of finger kinematics," *J. Biomech. Eng.*, vol. 147, no. 9, p. 091005, 2025.
- [30] Q. Zhang, T. Pi, R. Liu, and C. Xiong, "Simultaneous and proportional estimation of multijoint kinematics from emg signals for myoelectric control of robotic hands," *IEEE/ASME Trans. Mechatron.*, vol. 25, no. 4, pp. 1953–1960, 2020.
- [31] Z. Weng, Y. Xiao, P. Li, C. Yi, P. Bashivan, H. Ma, G. Yao, Y. Lin, F. Li, D. Yao, J. Hou, Y. Zhang, and P. Xu, "Real-time fine finger motion decoding for transradial amputees with surface electromyography," *Biomed. Signal Process. Control*, 2025.
- [32] I. Misra, C. L. Zitnick, and M. Hebert, "Shuffle and learn: Unsupervised learning using temporal order verification," in *ECCV*, 2016, pp. 527–544.
- [33] M. D. Li, K. Chang, B. Bearce, C. Y. Chang, A. J. Huang, J. P. Campbell, J. M. Brown, P. Singh, K. V. Hoebel, D. Erdogmus, S. Ioannidis, W. E. Palmer, M. F. Chiang, and J. Kalpathy-Cramer, "Siamese neural networks for continuous disease severity evaluation and change detection in medical imaging," *npj Digit. Med.*, vol. 3, p. 48, 2020.
- [34] M. Dong, L. Xie, S. R. Das, J. Wang, L. E. M. Wisse, R. deFlores, D. A. Wolk, and P. A. Yushkevich, "DeepAtrophy: Teaching a neural network to detect progressive changes in longitudinal MRI of the hippocampal region in Alzheimer's disease," *NeuroImage*, vol. 243, p. 118514, 2021.
- [35] H. Doughty, D. Damen, and W. Mayol-Cuevas, "Who's better? who's best? pairwise deep ranking for skill determination," in *CVPR*, 2018, pp. 6057–6066.
- [36] F. Feng, X. He, X. Wang, C. Luo, Y. Liu, and T.-S. Chua, "Temporal relational ranking for stock prediction," *ACM Trans. Inf. Syst.*, vol. 37, no. 2, p. 27, 2019.
- [37] A. Kendall, Y. Gal, and R. Cipolla, "Multi-task learning using uncertainty to weigh losses for scene geometry and semantics," in *CVPR*, 2018, pp. 7482–7491.
- [38] R. L. Lieber, M. D. Jacobson, B. M. Fazeli, R. A. Abrams, and M. J. Botte, "Architecture of selected muscles of the arm and forearm: anatomy and implications for tendon transfer," *J. Hand Surg. Am.*, vol. 17, no. 5, pp. 787–798, 1992.
- [39] O. Ronneberger, P. Fischer, and T. Brox, "U-net: Convolutional networks for biomedical image segmentation," in *MICCAI*, vol. 9351, 2015, pp. 234–241.
- [40] Z. Chen, Y. He, B. Li, H. Min, F. Sun, S. Li, and B. Fang, "A robotic prosthetic hand for computer mouse operations," *Adv. Intell. Syst.*, vol. 7, no. 5, p. 2500126, 2025.
- [41] R. S. Armiger and R. J. Vogelstein, "Air-guitar hero: A real-time video game interface for training and evaluation of dexterous upper-extremity neuroprosthetic control algorithms," in *IEEE Trans. Biomed. Circuits Syst.*, 2008, pp. 121–124.